Cell, Volume *137*

Supplemental Data

DEX-1 and DYF-7 Establish Sensory Dendrite Length by Anchoring Dendritic Tips during Cell Migration

Maxwell G. Heiman and Shai Shaham

SUPPLEMENTAL EXPERIMENTAL PROCEDURES

Constructing the *dex-1(ns42); dyf-7(ns117)* strain

The *dex-1(ns42); dyf-7(ns117)* strain was generated using the genetic balancer *hT2[qIs48],* a homozygous lethal translocation marked with *myo-2*pro:GFP, *pes-10*pro:GFP, and *ges-1*pro:GFP (Miskowski et al., 2001), to derive a strain of genotype *hT2[qIs48]/+* I*; hT2[qIs48]/dex-1(ns42)* III*; dyf-7(ns117)* X. When cultivated at 20°C, this strain showed 100% segregation of the *qIs48* GFP markers, implying that *dex-1(ns42)* III; *dyf-7(ns117)* X progeny were inviable. By cultivating this strain at 25°C, we recovered animals lacking the *qIs48* GFP markers that we inferred to be *dex-1(ns42)* III; *dyf-7(ns117)* X, and this genotype was confirmed by DNA sequencing.

dex-1 cDNA sequence

The *dex-1* cDNA clone yk679d4 (a gift of Yuji Kohara) was determined to contain additional exon sequence (underlined) not predicted in the WormBase database (http://wormbase.org) :

GGGGCTGTTAGTGTAGAAGAAGTTGATGACGTGGAAGTACTCCGAAGGGTGA
CAAGGACTATTGGAGAGAATTATAATGATCCAACATTTGTGGCGAAGAGTGC
TTTGGTGGTCACTTTTTCAAATGTTACTGATGGAAGACAGACGAAAGGA

dyf-7 linkage analysis and SNP mapping

dyf-7(m537) had previously been mapped to a 10.25 cM interval (between *dpy-6* (0 cM) and *unc-9* (10.25 cM)) on LG X (Starich et al., 1995). We generated a strain bearing *dyf-7(m537)* flanked by *dpy-6(e14)* and *unc-9(e101)* (Brenner, 1974) in the N2 background, crossed these animals to wild-type males of the CB4856 background, and performed single nucleotide polymorphism (SNP) mapping on Dpy nonUnc and Unc nonDpy recombinants, which refined the *dyf-7* position to a 0.7 cM interval (1.06 cM [SNP T20B5:4201] to 1.73 cM [SNP F19C6:30255] (Wicks et al., 2001)), corresponding to 21 cosmid clones.

dex-1 linkage analysis and SNP mapping

Using strains harboring mutations in defined LGs (MT3751, bearing *dpy-5(e61)* I; *rol-6(e187)* II; *unc-32(e189)* III, was generated by Jim Thomas; MT464, bearing *unc-5(e53)* IV; *dpy-11(e224)* V; *lon-2(e678)* X, was generated by Nancy Tsung and Robert Horvitz), we mapped *dex-1* to LG III. We then used SNP mapping to localize *dex-1* to a ~6.5 cM interval on LG III(–7.2 cM [SNP F45H7:3430964] (Swan et al., 2002) to –0.59 cM [SNP ZK686:8540] (Wicks et al., 2001)). We generated a strain bearing *dex-1(ns42)* flanked by *daf-2(m41)*(Larsen et al., 1995) and *unc-119(ed3)* (Brenner, 1974) and performed additional SNP mapping using Dex nonUnc and Dex nonDaf recombinants, which refined the *dex-1* position to a 0.4 cM interval (–1.69 cM [SNP W03A5:26463] to –1.30 cM [SNP C05D11:1800] (Wicks et al., 2001)), corresponding to 33 cosmid clones.

Bioinformatic analysis of the _dex-1_ interval

We used the programming language perl to search the *dex-1* interval for predicted proteins with putative transmembrane segments (using the MaxH segment-scoring method with Hopp-Woods hydrophilicity values (Boyd et al., 1998; Kyte and Doolittle, 1982)) and at least eight cysteines, a prerequisite for ZP domains. Of 420 predicted proteins, 27 had MaxH value >28 and at least eight cysteines, with *D1044.2* drawing our attention as a potential ZP-interactor due to its zonadhesin domain.

Measurements of axon length and cell body size

Axons were traced, rendered, and measured using the 3DModel module of Priism (http://www.msg.ucsf.edu/IVE/) (Chen et al., 1996). Cell bodies were traced and measured using the EditPolygon and VolumeBuilder modules.

Electron microscopy

Following standard methods (Lundquist et al., 2001), animals were fixed in glutaraldehyde and osmium tetroxide, cut open to aid infiltration of fixative and the embedding medium, embedded in Epon-Araldite, serially sectioned, and post-stained with uranyl acetate and lead citrate. Sections were imaged using a Tecnai G2 Spirit BioTwin transmission electron microscope (FEI) equipped with a 16-megapixel CCD digital camera (Gatan).

Optical cell marking

Embryos at late ball stage were picked to a drop of water, washed repeatedly to remove bacteria, and mounted on a 5% agar pad without azide. A 40x/1.35 NA objective was used to record the position of each embryo on the microscope stage, allowing for rapid revisiting of all embryos at higher magnification. With the 100x objective in place, the Quantifiable Laser Module was then aligned, and embryos were quickly revisited to identify early bean stage embryos with their dorsal sides facing the cover glass. To identify the position of the neuron of interest and to define the limits of the focal stack, ~10 images of <1 sec each of the green Kaede fluorescence (excitation 470/40 nm, emission 525/50 nm) were acquired at different focal planes. An additional ultraviolet-blocking filter was found to be critical to prevent phototoxic arrest of embryonic development and nonspecific photoconversion of Kaede. The laser was targeted to the medial anterior boundary of the cell of interest, as far as possible from other Kaede-

expressing cells due to the fact that the laser photoconverts Kaede anywhere along its path, including cells in adjacent focal planes (it was unavoidable that some cells outside the ~5-µm-thick region of interest were inadvertantly photoconverted).

At each time point, acquisition of each stack took about 1.5 min, with fluorescence exposure times of ~5 sec per optical section, equivalent to ~1 min per stack; however, exposure to the green excitation light used to visualize photoconverted Kaede did not result in appreciable nonspecific photoconversion or developmental arrest. Between time points the focal midpoint of the stack was adjusted to compensate for rotation of the embryo and movement of the cell of interest.

Notes on image processing

Projections were adjusted for brightness, contrast and false-color intensity indexing using Photoshop 7 (Adobe Software); gamma values were held at 1. Merged color images were assembled using the "Screen" layer mode in Photoshop.

Quantitative analysis of cell migration

Maximum brightness projections of time-lapse images were rotated so that the long axis of the eggshell was oriented along the vertical axis of the frame, as shown in Fig. 3. The vertical axis positions (y) of the dendritic tip, nucleus, and leading edge of the cell were subjectively identified at each time point (t). Due to differences in the initiation of each time course and how each embryo was positioned, this resulted in cell migration plots offset from each other by arbitrary values in space and time. To shift these plots into register, velocity of the nucleus over 20-min intervals was calculated for each time point "i" as $[(y_{t=i+20} - y_{t=i}) \div 20]$ and the vertical axis position and time index when the velocity crossed zero (i.e., the place and time when the migration of the nucleus ended) were defined as [(y,t) = (0,0)] for all plots.

Mosaic analysis of *dex-1* and *dyf-7* function

Mosaic analysis was performed using *dex-1(ns42)* and *dyf-7(m537)* animals bearing unstable extrachromosomal transgene arrays consisting of rescuing cosmids (D1044 or C43C3, respectively) and markers of individual amphid lineages, as follows: *F16F9.3*pro:GFP (amphid sheath glial cell (AmSh)); *str-1*pro:mCherry (AWB); *odr-1*pro:GFP (AWB and AWC); *gcy-8*pro:RFP (AFD). This strategy rendered the four amphid lineages easily discernable by fluorescence and morphology: green sheath, ABpl/raapa (includes AmSh, AWA, ASG, ASI); green neuron, ABpl/rpaa (includes amphid socket glial cell, AWC, ASH); yellow neuron, ABalpppp/ABpraaap (includes AWB, ASE, ADF, ASJ, ADL); red neuron, ABalpppap/ABpraaaap (includes AFD, ASK).

Due to partial penetrance of *dex-1(ns42),* only phenotypically Dex animals bearing the extrachromosomal array were informative. Of 245 individuals examined, 77 did not express the array markers in any amphid lineage; 123 expressed the array markers in all amphid lineages; and 45 were amphid mosaics. Of the latter, only two were phenotypically Dex; extensive further screening identified one additional mosaic Dex animal. Of these animals, one carried the array only in the AWB lineage; one carried the array in all lineages but AWB; and one carried the array in the AmSh and AWC lineages.

Similarly, in *dyf-7(m537)*, mosaic animals expressing the Dex phenotype were very rare. NonDex amphid mosaics were identified bearing the array in almost every combination of amphid lineages, and the rare Dex mosaics we identified did not exhibit loss of the array in a common lineage.

Cell culture

Drosophila Schneider (S2) cells (Invitrogen) were cultured at 25°C according to the distributor's instructions, in Shields and Sang M3 insect medium (Sigma) supplemented with fetal bovine serum, penicillin, and streptomycin. For transfections, logarithmically growing cells were plated at a density of 10^6 cells/ml in 2 ml medium and the next day were transfected using 1 µg plasmid DNA which had been incubated for 15 min at room temperature with 8 µl FuGene HD transfection reagent (Roche) in 100 µl Opti-MEM I medium (Invitrogen).

Protein analysis

Two days after transfections, cells were resuspended by pipetting, 1 ml of cells in conditioned medium was collected, cells were pelleted at ~2000 rcf for 30 sec, the supernatant conditioned medium was collected (340 µl), the cell pellet was washed 3x with fresh medium, cells were resuspended in 1 ml fresh medium and the cell suspension was collected (340 µl). Samples were mixed with 160 µl concentrated lysis buffer to obtain 500 µl of sample in loading buffer with a final concentration of 60 mM Tris HCl pH 8.0, 2% sodium dodecyl sulfate (SDS), 10% glycerol, 5% β-mercaptoethanol, 0.01% bromophenol blue, and 1x Complete protease inhibitor cocktail (Roche). Samples were boiled 3 min, cell lysates were passed 3x quickly through a 25 G needle (Becton Dickinson) to shear genomic DNA. For non-reduced samples, β-mercaptoethanol was omitted and samples were heated at 50°C instead of boiled. Samples were immediately centrifuged at 16,000 rcf for 2 min and loaded (15 µl per lane) on NuPage 4-12% Bis-Tris pre-cast gels (Invitrogen), except for the DEX-1ΔTM C-terminal myc tag which, due its greater reactivity compared to the DEX-1 C-terminal myc tag, was diluted 1:20. Samples were electrophoresed and transferred to polyvinylidene difluoride (PVDF) membrane (Bio-Rad), and immunoblotting was performed in PBST (1x phosphate buffered saline (Roche) with 0.05% Tween-20 (Bio-Rad)) with 5% milk using antibodies as in Methods. Reactivity was detected with Western Lightning chemiluminescence reagent (PerkinElmer). For fluorescence detection (Supp. Fig. 6), immunoblots were performed using Odyssey Blocking Buffer (LiCor), rat monoclonal anti-HA 3F10 (Roche) 1:4000 and goat polyclonal anti-rat IgG coupled to IRDye 800CW (LiCor) 1:4000, and were detected with an Odyssey Infrared Imager (LiCor).

For immunoprecipitation, 500 µl transfected cells were pelleted at ~2000 rcf for 30 sec, resuspended in 1 ml IP buffer, and rotated at 4°C for 30 min. Meanwhile, 75 µl anti-myc agarose slurry was washed four times for 5 min each in 1 ml IP buffer. Lysate was centrifuged at 16,000 rcf for 5 min, input sample (IN) was collected, and 150 µl of lysate was added to 75 µl of anti-myc agarose. Immunoprecipitation was performed at 4°C for 2 h, after which time an unbound (UB) fraction was collected, agarose was washed three times in 1 ml IP buffer, and washed agarose was suspended in 150 µl IP buffer (IP). The IN, UB, and IP fractions were supplemented to final concentrations of 2% SDS and 0.01% bromophenol blue, heated at 50°C for 5 min, and analyzed as above. Samples

were loaded at volumes of 8.2 µl IN, 10 µl UB, 8.2 µl IP to normalize their relative dilutions, and analyzed by immunoblot as above.

SUPPLEMENTAL REFERENCES

Adler, C.E., Fetter, R.D. and Bargmann, C.I. (2006) UNC-6/Netrin induces neuronal asymmetry and defines the site of axon formation. *Nat Neurosci*, **9**, 511-518.

Ando, R., Hama, H., Yamamoto-Hino, M., Mizuno, H. and Miyawaki, A. (2002) An optical marker based on the UV-induced green-to-red photoconversion of a fluorescent protein. *Proc Natl Acad Sci U S A*, **99**, 12651-12656.

Bacaj, T., Tevlin, M., Lu, Y. and Shaham, S. (2008) Glia are essential for sensory organ function in C. elegans. *Science*, **322**, 744-747.

Boyd, D., Schierle, C. and Beckwith, J. (1998) How many membrane proteins are there? *Protein Sci*, **7**, 201-205.

Brenner, S. (1974) The genetics of Caenorhabditis elegans. *Genetics*, **77**, 71-94.

Chen, H., Hughes, D.D., Chan, T.A., Sedat, J.W. and Agard, D.A. (1996) IVE (Image Visualization Environment): a software platform for all three-dimensional microscopy applications. *J Struct Biol*, **116**, 56-60.

Corpet, F. (1988) Multiple sequence alignment with hierarchical clustering. *Nucleic Acids Res*, **16**, 10881-10890.

Finn, R.D., Mistry, J., Schuster-Bockler, B., Griffiths-Jones, S., Hollich, V., Lassmann, T., Moxon, S., Marshall, M., Khanna, A., Durbin, R., Eddy, S.R., Sonnhammer, E.L. and Bateman, A. (2006) Pfam: clans, web tools and services. *Nucleic Acids Res*, **34**, D247-251.

Gower, N.J., Temple, G.R., Schein, J.E., Marra, M., Walker, D.S. and Baylis, H.A. (2001) Dissection of the promoter region of the inositol 1,4,5-trisphosphate receptor gene, itr-1, in C. elegans: a molecular basis for cell-specific expression of IP3R isoforms. *J Mol Biol*, **306**, 145-157.

Han, K., Levine, M.S. and Manley, J.L. (1989) Synergistic activation and repression of transcription by Drosophila homeobox proteins. *Cell*, **56**, 573-583.

Horner, M.A., Quintin, S., Domeier, M.E., Kimble, J., Labouesse, M. and Mango, S.E. (1998) pha-4, an HNF-3 homolog, specifies pharyngeal organ identity in Caenorhabditis elegans. *Genes Dev*, **12**, 1947-1952.

Kyte, J. and Doolittle, R.F. (1982) A simple method for displaying the hydropathic character of a protein. *J Mol Biol*, **157**, 105-132.

Landmann, F., Quintin, S. and Labouesse, M. (2004) Multiple regulatory elements with spatially and temporally distinct activities control the expression of the epithelial differentiation gene lin-26 in C. elegans. *Dev Biol*, **265**, 478-490.

Lanjuin, A., Claggett, J., Shibuya, M., Hunter, C.P. and Sengupta, P. (2006) Regulation of neuronal lineage decisions by the HES-related bHLH protein REF-1. *Dev Biol*, **290**, 139-151.

Larsen, P.L., Albert, P.S. and Riddle, D.L. (1995) Genes that regulate both development and longevity in Caenorhabditis elegans. *Genetics*, **139**, 1567-1583.

Lundquist, E.A., Reddien, P.W., Hartwieg, E., Horvitz, H.R. and Bargmann, C.I. (2001) Three C. elegans Rac proteins and several alternative Rac regulators control axon

guidance, cell migration and apoptotic cell phagocytosis. *Development*, **128**, 4475-4488.

Maduro, M. and Pilgrim, D. (1995) Identification and cloning of unc-119, a gene expressed in the Caenorhabditis elegans nervous system. *Genetics*, **141**, 977-988.

Mello, C.C., Kramer, J.M., Stinchcomb, D. and Ambros, V. (1991) Efficient gene transfer in C.elegans: extrachromosomal maintenance and integration of transforming sequences. *Embo J*, **10**, 3959-3970.

Miskowski, J., Li, Y. and Kimble, J. (2001) The sys-1 gene and sexual dimorphism during gonadogenesis in Caenorhabditis elegans. *Dev Biol*, **230**, 61-73.

Okkema, P.G., Harrison, S.W., Plunger, V., Aryana, A. and Fire, A. (1993) Sequence requirements for myosin gene expression and regulation in Caenorhabditis elegans. *Genetics*, **135**, 385-404.

Spieth, J., Brooke, G., Kuersten, S., Lea, K. and Blumenthal, T. (1993) Operons in C. elegans: polycistronic mRNA precursors are processed by trans-splicing of SL2 to downstream coding regions. *Cell*, **73**, 521-532.

Starich, T.A., Herman, R.K., Kari, C.K., Yeh, W.H., Schackwitz, W.S., Schuyler, M.W., Collet, J., Thomas, J.H. and Riddle, D.L. (1995) Mutations affecting the chemosensory neurons of Caenorhabditis elegans. *Genetics*, **139**, 171-188.

Swan, K.A., Curtis, D.E., McKusick, K.B., Voinov, A.V., Mapa, F.A. and Cancilla, M.R. (2002) High-throughput gene mapping in Caenorhabditis elegans. *Genome Res*, **12**, 1100-1105.

Troemel, E.R., Sagasti, A. and Bargmann, C.I. (1999) Lateral signaling mediated by axon contact and calcium entry regulates asymmetric odorant receptor expression in C. elegans. *Cell*, **99**, 387-398.

Verhoeven, K., Van Laer, L., Kirschhofer, K., Legan, P.K., Hughes, D.C., Schatteman, I., Verstreken, M., Van Hauwe, P., Coucke, P., Chen, A., Smith, R.J., Somers, T., Offeciers, F.E., Van de Heyning, P., Richardson, G.P., Wachtler, F., Kimberling, W.J., Willems, P.J., Govaerts, P.J. and Van Camp, G. (1998) Mutations in the human alpha-tectorin gene cause autosomal dominant non-syndromic hearing impairment. *Nat Genet*, **19**, 60-62.

Wicks, S.R., Yeh, R.T., Gish, W.R., Waterston, R.H. and Plasterk, R.H. (2001) Rapid gene mapping in Caenorhabditis elegans using a high density polymorphism map. *Nat Genet*, **28**, 160-164.

Yu, S., Avery, L., Baude, E. and Garbers, D.L. (1997) Guanylyl cyclase expression in specific sensory neurons: a new family of chemosensory receptors. *Proc Natl Acad Sci U S A*, **94**, 3384-3387.

TABLE S1

Transgenes used in this study

A. Stably integrated transgenes

allele	linkage group (LG)	construct(s)	reference
nsIs53	IV	pMH1	this study
kyIs136	X	*str-2*pro:GFP, *lin-15(+)*	(Troemel et al., 1999)
ntIs1	V	*gcy-5*pro:GFP, *lin-15(+)*	(S. Lockery, unpublished; Yu et al., 1997)
oyIs44	V	*odr-1*pro:RFP, *lin-15(+)*	(P. Sengupta, unpublished)
oyIs45	V	*odr-1*pro:YFP, *lin-15(+)*	(P. Sengupta, unpublished)
oyIs51	V	*srh-142*pro:RFP, *lin-15(+)*	(Lanjuin et al., 2006)
nsIs96	I	pMH22, pDP#MM051	this study

B. Unstable extrachromosomal transgenes. These alleles were generated as part of this study.

allele(s)	constructs
nsEx1153, nsEx2073	pMH2, pMH3, pRF4
nsEx2095	pMH4, pRF4
nsEx2135	pMH5, pRF4
nsEx1493	pMH6, pRF4
nsEx1333, nsEx1334, nsEx1368	pMH7, pRF4
nsEx1480, nsEx1481, nsEx1483	pMH8, pRF4
nsEx1468, nsEx1469, nsEx1471, nsEx2452, nsEx2453, nsEx2454	pMH9, pRF4
nsEx1472, nsEx1473, nsEx1475	pMH10, pRF4
nsEx1988, nsEx2007, nsEx2008	pMH11, pRF4
nsEx2023, nsEx2024, nsEx2050	pMH12, pRF4
nsEx1974, nsEx1975, nsEx1976	pMH13, pRF4
nsEx1835, nsEx1836, nsEx2458	pMH14, pRF4
nsEx1142, nsEx1145, nsEx1146, nsEx2455, nsEx2456, nsEx2457	pMH15, pRF4
nsEx1437, nsEx1439, nsEx1451	pMH16, pRF4
nsEx2025, nsEx2026, nsEx2051	pMH17, pRF4
nsEx1229, nsEx1230, nsEx1231	pMH18, pRF4
nsEx1996, nsEx1997, nsEx1998	pMH19, pRF4
nsEx2070, nsEx2133, nsEx2134	pMH20, pRF4
nsEx1755, nsEx1820, nsEx1845	pMH21, pRF4
nsEx2459, nsEx2460	pMH29, pRF4
nsEx2325, nsEx2461	pMH28, pMH29, pRF4
nsEx2451	pTB78, pRF4

TABLE S2

Plasmids used in this study

DNA sequences are available at http://shahamlab.rockefeller.edu/publications

Plasmid	Description	Notes
pMH1	*vap-1*pro:RFP:*unc-119*	*vap-1*pro a gift of Leo Liu, *unc-119* see (Maduro and Pilgrim, 1995)
pMH2	*F16F9.3*pro:mCherry	*F16F9.3*pro a gift of Maya Tevlin, (Bacaj et al., 2008)
pMH3	*itr-1*pro:CFP	*itr-1*pro a gift of Howard Baylis, see (Gower et al., 2001)
pMH4	*dex-1*pro:*dex-1*-mCherry	mCherry inserted at engineered 3' NotI site, see pMH7
pMH5	*dyf-7*pro:*dyf-7*-GFP	GFP fused at 3' site corresponding to fusion after C-terminal VDS in protein sequence
pMH6	*gcy-5*pro:mCherry:SL2:*dyf-7*-GFP	*gcy-5*pro after (Yu et al., 1997); SL2 a gift of Maya Goldmit, see (Spieth et al., 1993)
pMH7	*dex-1*pro:*dex-1*	*dex-1* cDNA, yk679d4, a gift of Yuji Kohara. NotI restriction site was engineered at 3' appending peptide AAA at protein C-terminus
pMH8	*pha-4*pro:*dex-1*	*pha-4*pro a gift of Susan Mango, see (Horner et al., 1998)
pMH9	*dyf-7*pro:*dex-1*	
pMH10	*lin-*26e1:*myo-2*minpro:*dex-1*	*lin-26*e1 after (Landmann et al., 2004); *myo-2*minpro after (Okkema et al., 1993)
pMH11	*dex-1*pro:*dex-1*ΔTM	*dex-1*ΔTM deletes sequences 3' to *agtacaactcaa*, truncating the protein after STTQ, but retains 3' engineered NotI site
pMH12	*dyf-7*pro:*dex-1*ΔTM	See pMH11
pMH13	*lin-26*e1:*myo-2*minpro:*dex-1*ΔTM	See pMH10, pMH11
pMH14	*dyf-7*pro:DEX-1-DYF-7	DEX-1 extracellular domain-coding sequences (AARL…QSTT) inserted at engineered AgeI site in *dyf-7* cDNA (*gatcgattt* to *gaccggttt)* corresponding to insertion after EKDR in DYF-7 protein sequence
pMH15	*dyf-7*pro:*dyf-7*	*dyf-7* cDNA, yk663, a gift of Yuji Kohara
pMH16	*pha-4*pro:*dyf-7*	See pMH8

pMH17	*dex-1*pro:*dyf-7*	
pMH18	*lin-26*e1:*myo-2*minpro:*dyf-7*	See pMH10
pMH19	*dyf-7*pro:*dyf-7*ΔCFCS	*dyf-7*ΔCFCS is a deletion-insertion replacing 193 bp (*cgtctgcgt…agcaaagaa*) with 13 bp (*accatggacctagga)*, at the protein level replacing the arginine-rich RLRFRHKR...QRR with TMDLG
pMH20	*dex-1*pro:*dyf-7*ΔCFCS	see pMH19
pMH21	*lin-26*e1:*myo-2*minpro:*dyf-7*ΔCFCS	*lin-26*e1 after (Landmann et al., 2004); *myo-2*minpro after (Okkema et al., 1993)
pMH22	*dyf-*7pro:Kaede	Kaede from pKaede-S1 (MBL, Intl.), see (Ando et al., 2002)
pMH23	*Ac:*FLAG-*dex-1*-myc	pAc*, Drosophila* actin 5c promoter vector, a gift of Kang Shen; see (Han et al., 1989). For epitope insertions see pMH14
pMH24	*Ac:*FLAG-*dex-1*ΔTM-myc	See pMH23 and pMH14
pMH25	*Ac:*HA-*dyf-7*-FLAG	See pMH23 and pMH14. HA inserted at engineered silent AgeI site. FLAG inserted at 3' and replacing C-terminal LYR
pMH26	*Ac:*HA-*dyf-7*ΔCFCS-FLAG	See pMH23, pMH19, pMH25
pMH27	*Ac:*HA-DYF-7(V52E)ΔCFCS-FLAG	See pMH23, pMH19, pMH25
pMH28	*dex-1*pro:myristyl-mCherry	Myristylation sequence MGSCIGK (Adler et al., 2006) inserted at N-terminus of mCherry
pMH29	*dyf-7*pro:myristyl-GFP	Myristyl-GFP from (Adler et al., 2006)
pMH30	*Ac:*HA-DYF-7(V191D)ΔCFCS-FLAG	See pMH23, pMH19, pMH25
pRF4	*rol-6(su1006)*	(Mello et al., 1991)
pDP#MM051	*unc-119(+)*	(Maduro and Pilgrim, 1995)
pTB78	*odr-1*pro:*odr-10*-GFP	(Bacaj et al., 2008)

TABLE S3

dex-1 and *dyf-7* mutations

Substitutions and insertions are bracketed with the mutant sequence underlined. Upper-case corresponds to predicted exons; lower-case to predicted introns.

Allele	Sequence
dex-1(ns42)	AGACCC[C>T]GACCAA
dyf-7(m537)	GTCTAC[ATTTATGGTCATTTATGGTCAGTATGGTCATTTATGGTCATT TATGGTCATTTATGGTCATTTATGGTCATATGGTCTAC]GTTTAT
dyf-7(ns88)	GACAGA[G>A]AAGATA
dyf-7(ns116)	AATTTG[T>A]TGAATT
dyf-7(ns117)	ctttag[C>T]CTAAAC
dyf-7(ns118)	CCGCAG[G>A]CGCTGC
dyf-7(ns119)	ATGAAT[C>T]AATTGT
dyf-7(ns120)	CCGAAG[T>A]AATGAG

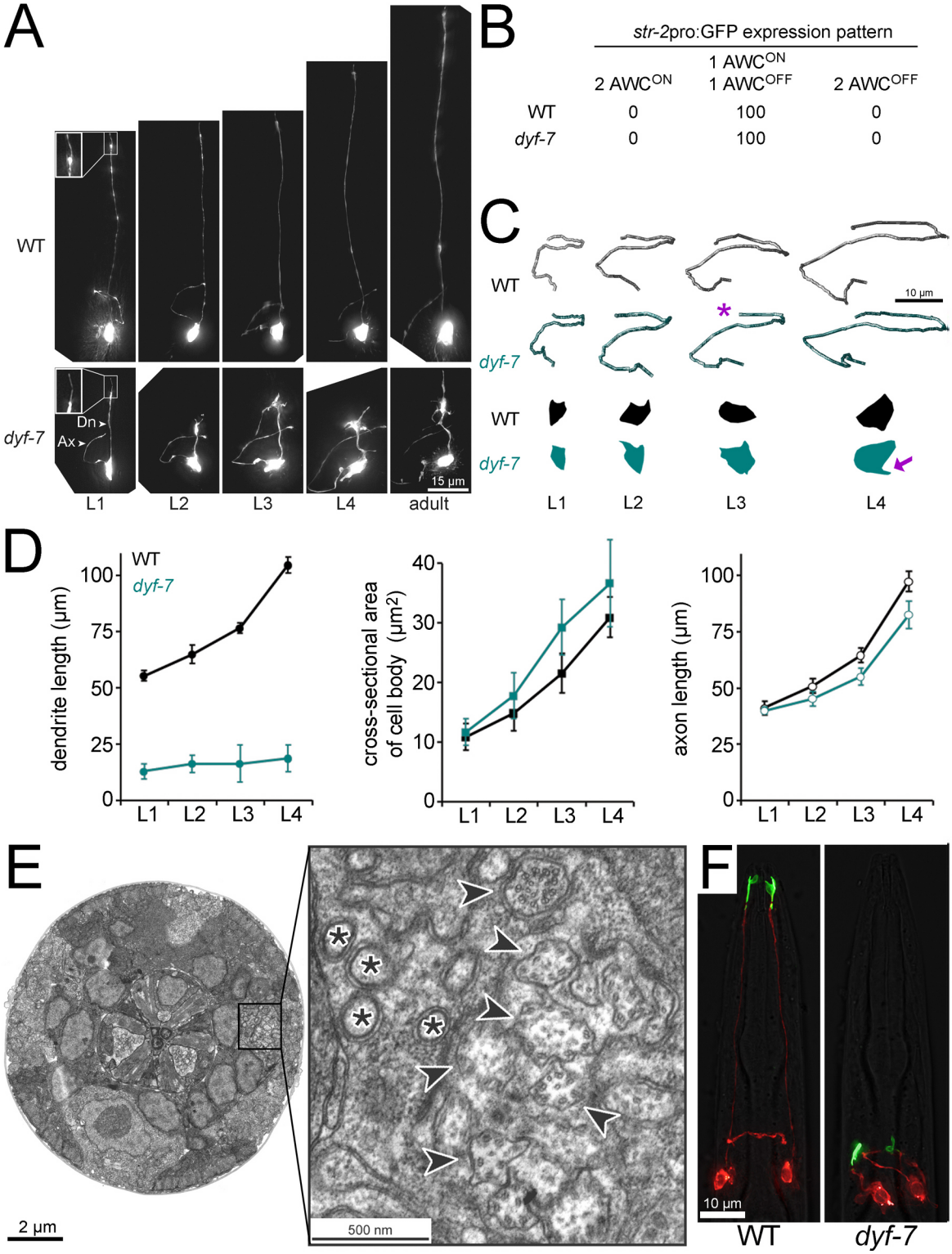

FIGURE S1. Amphid scaling and ultrastructure in *dyf-7* animals

A, WT and *dyf-7(m537)* animals expressing *gcy-5*pro:GFP (ASER neuron) were imaged at each larval stage and as adults. Despite the dendrite extension defect, the *dyf-7*

L1 neuron displays a sensory cilium comparable to that seen in WT (inset, 2x magnification). During larval growth, *dyf-7* dendrites appear to increase in volume and surface area without increasing in length. Ax, axon; Dn, dendrite. B, WT and *dyf-7(m537)* animals were examined for expression of *str-2*pro:GFP. Normal expression of *str-2*pro:GFP in either but not both of AWCL and AWCR requires axonal contacts between these neurons and is disrupted in mutants that affect axon guidance (Troemel et al., 1999). n=100 for each genotype. C, Axon morphology and cell body cross-sections of ASER in WT or *dyf-7(m537)* animals expressing *gcy-5*pro:GFP were traced at each larval stage. Anterior is at top; for axon tracings, connection to the cell body is at bottom. Some *dyf-7* axons display a modest premature termination defect (asterisk) and some cell bodies display additional protrusions (arrow). D, Dendrite lengths, cell body cross-sectional areas, and axon lengths of WT or *dyf-7(m537)* animals were measured at each larval stage. n=10 for each genotype at each stage. Error bars, standard deviation. E, Electron micrograph of a cross-section taken slightly anterior to the nerve ring of a *dyf-7(m537)* L1 animal, showing an apparently intact bundle of amphid sensory cilia (arrowheads) and "fingers" (asterisks) typical of the modified cilium of the AFD neuron. Membranes of the sheath glial cell are visible forming the channel in which the sensory cilia lie, and ensheathing individual AFD fingers. F, Localization of the ciliary odorant receptor ODR-10 in AWC neurons of WT and *dyf-7(m537)* animals was visualized using *odr-1*pro:*odr-10*-GFP and *odr-1*pro:RFP transgenes to co-express ODR-10-GFP (green) and soluble cytoplasmic RFP (red).

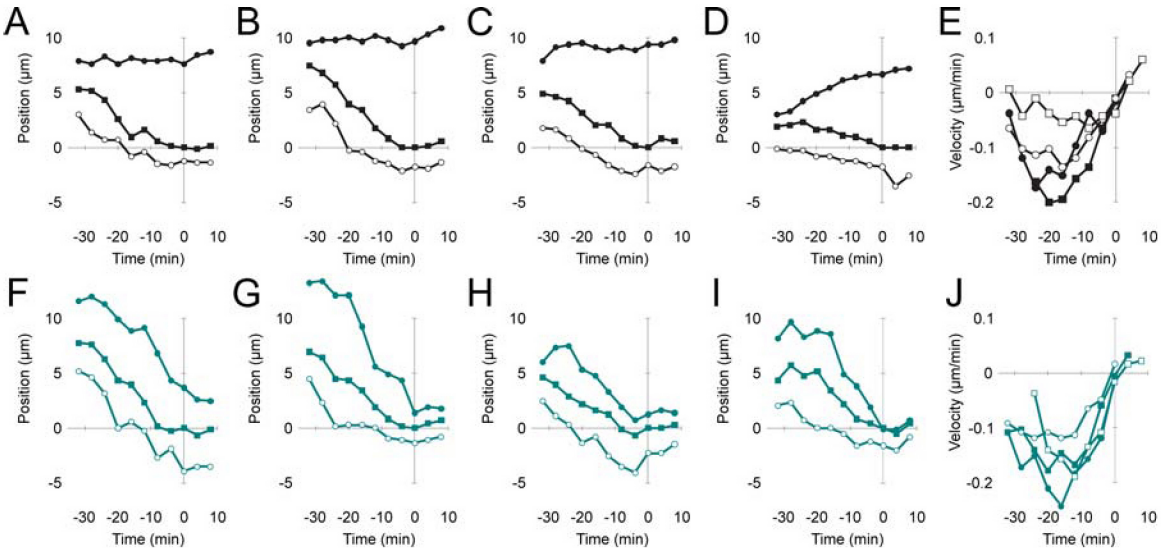

FIGURE S2. Quantitative analysis of neuron cell body migration

A-D, The vertical axis positions over time of the dendritic tip (closed circles), nucleus (squares), and leading edge (open circles) of migrating neurons in the WT embryos shown in Movies 2-5, respectively. Apparent anterograde movement of dendritic tip in D is due to earlier onset of overall embryo elongation and rotation while the dendritic tip remained stationary relative to its surroundings, not due to growth cone crawling (see Movie 5). E, Velocity of nucleus movement, measured over 20 min intervals, in the embryo shown in Movie 2 (closed circles), 3 (closed squares), 4 (open circles), and 5 (open squares). F-J, Same as A-E but corresponding to *dyf-7(m537)* embryos shown in Movies 6-9.

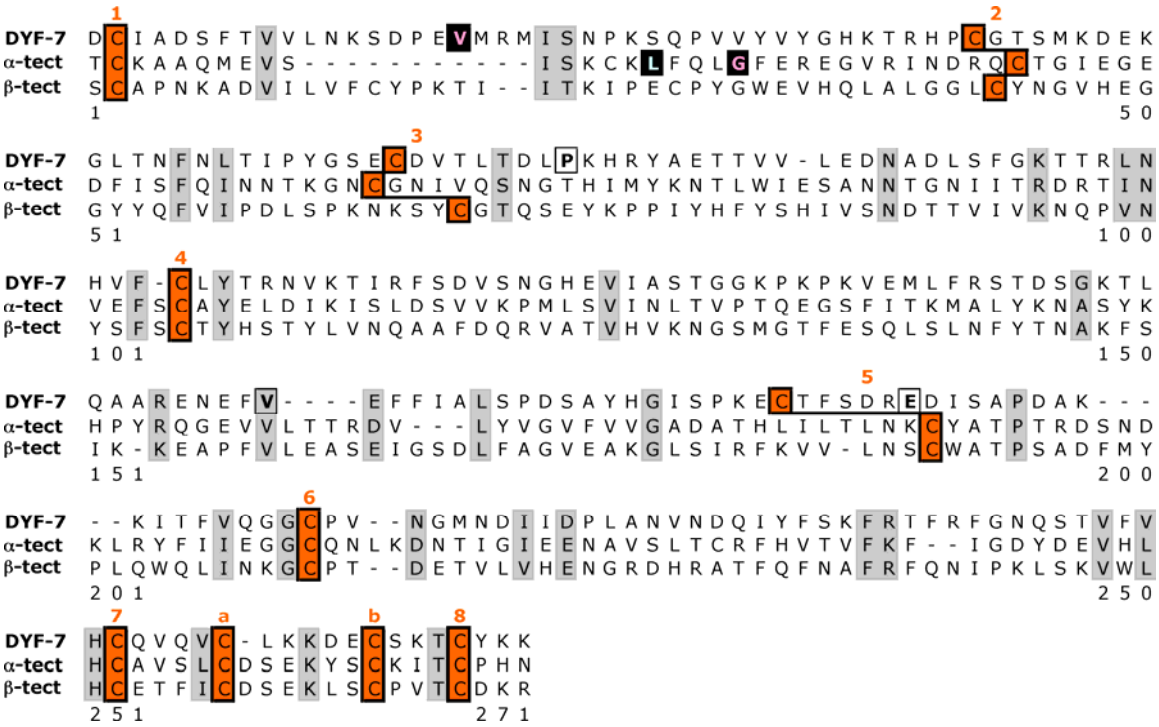

FIGURE S3. Alignment of DYF-7 and tectorin ZP domains

ZP domains, as identified by Pfam (Finn et al., 2006), of DYF-7 and human α-tectorin and β-tectorin proteins were aligned by MultAlin (Corpet, 1988). The strongly penetrant DYF-7(V52E) mutation corresponds well in region and chemistry to α-tectorin(G1824D), which is found together with α-tectorin(L1820F) in familial deafness (Verhoeven et al., 1998) (black background). Orange boxes, conserved cysteines that define the ZP domain; grey, other conserved residues; bold boxed letters, other DYF-7 point mutations in the ZP domain that disrupt dendrite anchoring.

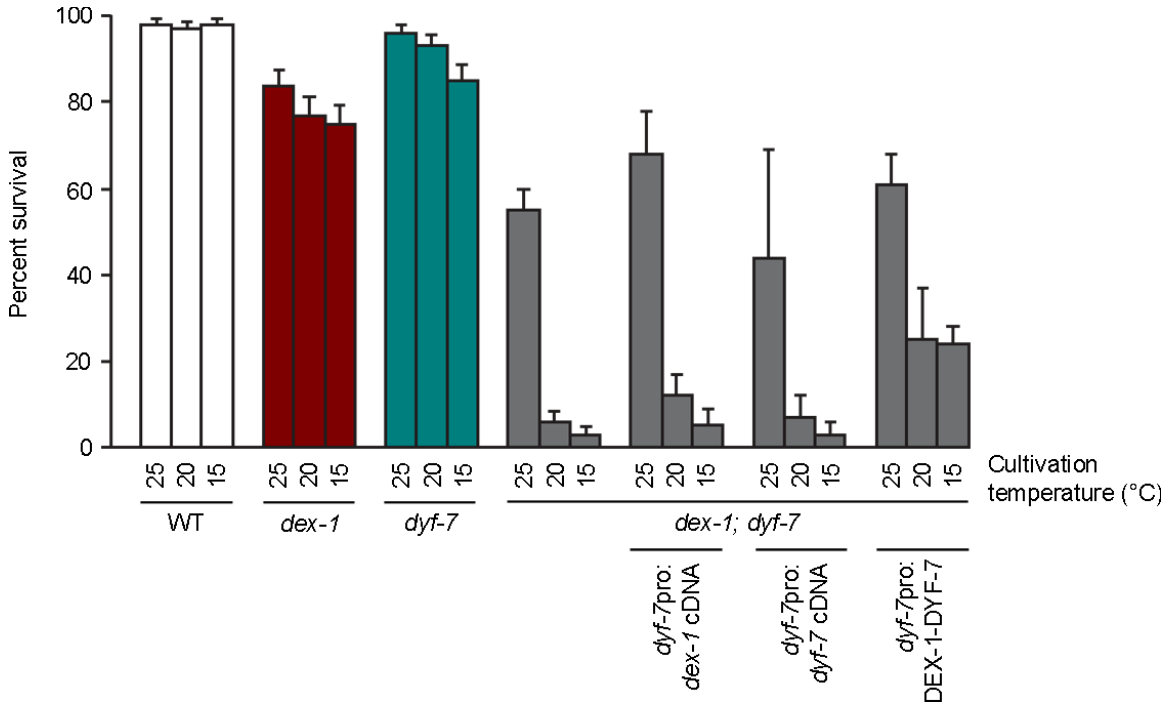

FIGURE S4. Rescue of the *dex-1*; *dyf-7* mutant using a DEX-1-DYF-7 fusion protein

Animals bearing *dex-1(ns42)*, *dyf-7(ns117),* both, or neither, and bearing transgenes consisting of the *dyf-7* promoter driving the *dex-1* or *dyf-7* cDNA or a DEX-1-DYF-7 fusion gene were assayed for viability as follows. 25 fourth larval stage (L4) animals were cultivated at 25°C, 20°C, or 15°C for 1, 2, or 4 d, respectively, at which point 100 embryos were picked to fresh plates at the same temperature. After an additional 2, 4, or 6 d, respectively, the numbers of animals that had developed past the second larval stage (L2) were counted. Error bars, standard errors of the means for strains without rescuing transgenes; standard deviations among three independent transgenic lines for strains with rescuing transgenes.

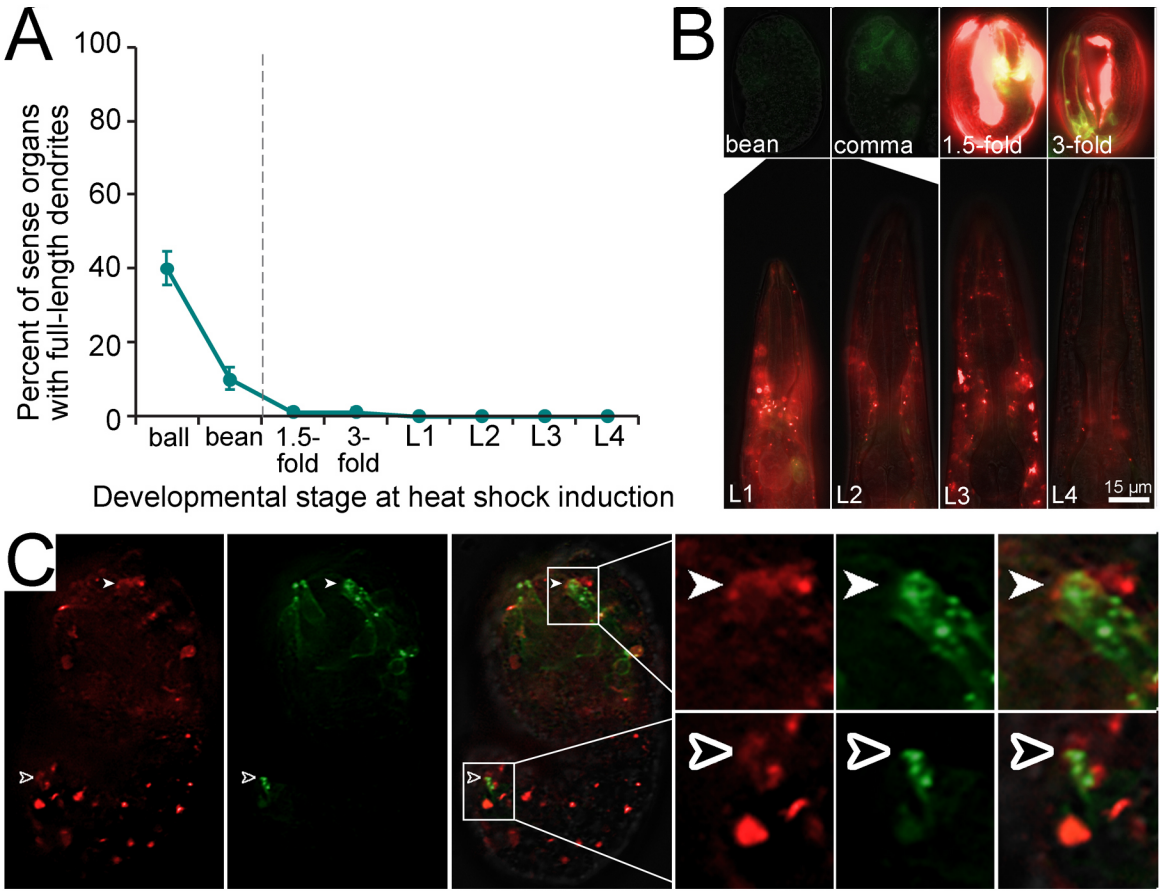

FIGURE S5. Timing and localization of DYF-7 and DEX-1

A, *dyf-7(m537)* animals bearing the *dyf-7* cDNA transgene under control of heat-shock-inducible promoters (a mixture of *hsp16-2*pro:*dyf-7* cDNA and *hsp16-41*pro:*dyf-7* cDNA) were subjected to heat shock (30 min at 34°C) at the indicated developmental stages, and dendrite lengths scored in adults. Error bars, standard errors of the means. B, Animals expressing *dex-1*pro:myristyl-mCherry and *dyf-7*pro:myristyl-GFP transgenes were imaged at each developmental stage under fixed exposure conditions. Brightness and contrast of each image were adjusted identically. Single focal planes are shown. C, An embryo expressing *dex-1*pro:*dex-1*-mCherry and *dyf-7*pro:*dyf-7*-GFP transgenes was imaged at the conclusion of dendrite extension. Green fluorescence, red fluorescence, and a merged fluorescence and transmitted light image of a single focal plane are shown (left to right). A cap of DEX-1-mCherry staining is visible surrounding the punctate DYF-7-GFP staining at dendritic tips in the amphid (closed arrowhead) and the phasmid (open arrowhead), a functionally analagous structure in the tail that is also affected by *dyf-7(m537)* (Starich et al., 1995). Other foci of DEX-1-mCherry and DYF-7-GFP expression do not colocalize.

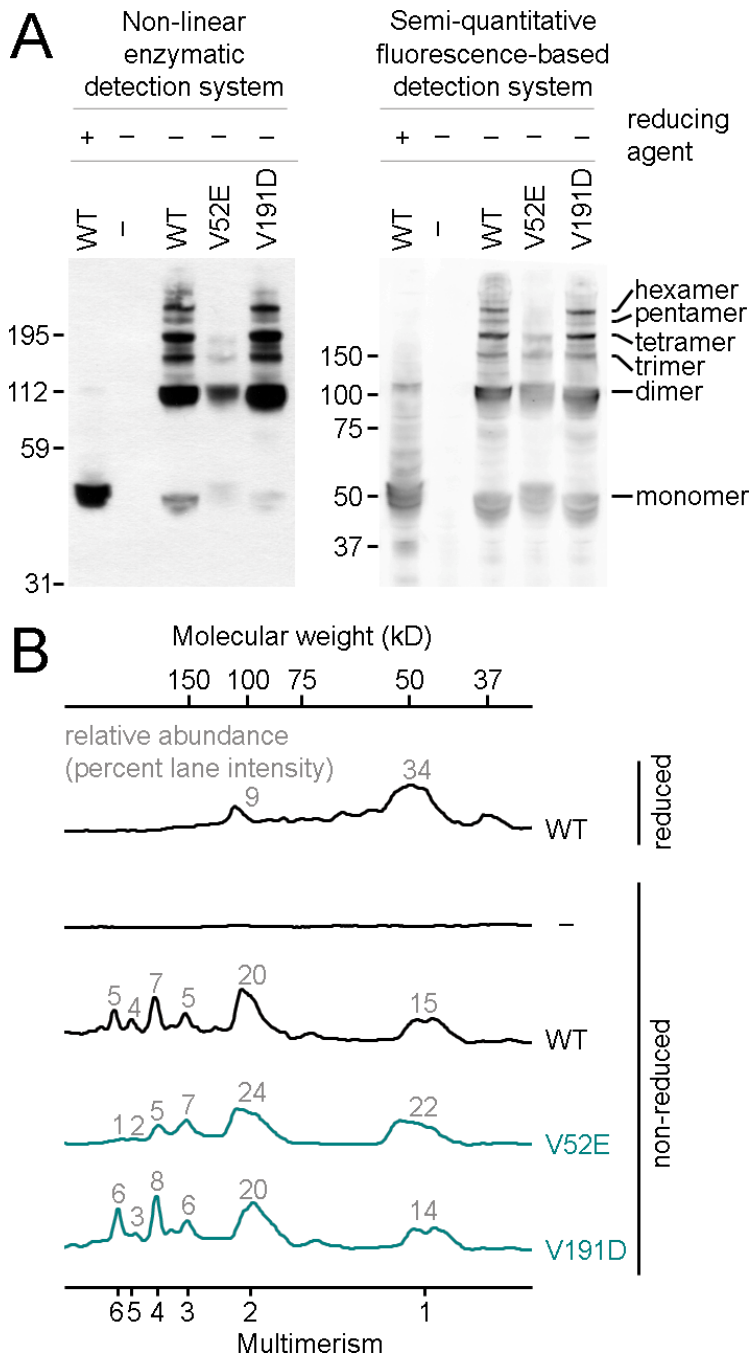

FIGURE 6. Quantitative analysis of DYF-7 multimerization

A, S2 insect cells were transfected, or not (–), with HA-DYF-7ΔCFCS-FLAG (WT) or the same construct bearing the V52E or V191D mutation. Cell lysates were collected under reducing (5% β-mercaptoethanol (β-me), boiling) or nonreducing (no β-me, 50°C) conditions. Samples were split and analyzed by anti-HA immunoblot using both an enzymatic amplification detection system and a fluorescence detection system designed to produce a signal response that remains linear over several orders of magnitude. B, Profiles of signal intensities obtained using the direct fluorescence detection system were analyzed using ImageJ (http://rsbweb.nih.gov/ij/) and normalized to total lane intensity.